Impact of Renewable Distributed Generation on Power Systems

M. Begović, A. Pregelj, A. Rohatgi
School of Electrical and Computer Engineering
Georgia Institute of Technology
Atlanta, GA 30332-0250

D. Novosel
ABB T&D Technology Ltd
Baden, Switzerland

Abstract

The traditional approach in electric power generation is to have centralized plants distributing electricity through an extensive transmission & distribution network. Distributed generation (DG) provides electric power at a site closer to the customer, eliminating the unnecessary transmission and distribution costs. In addition, it can reduce fossil fuel emissions, defer capital cost, reduce maintenance investments and improve the distribution feeder voltage conditions. In the case of small residential photovoltaic (PV) and wind systems, the actual generator locations and DG penetration level are usually not apriori known. The following study attempts to calculate the boundaries of the impact of randomly placed distributed generators on a distribution feeder. Monte Carlo simulations are performed, and boundaries for overall improvements are determined. The study shows that the knowledge of total penetration of small PV systems is sufficient to estimate the effects of DG on the feeder.

1. Introduction

This paper investigates the effects of the dispersed generation (DG) devices onto the electric power distribution system. The prevailing utility strategy, so far, is to treat the DG devices as a parasitic source, and to impose a set of strict rules designed to limit the effects that those systems may have on the distribution feeder. The reasoning for these actions is simple. Most US utilities are currently price regulated, which simply means that the actual utility's revenues (and profits) are dictated entirely by sales. DG devices installed at the customer level reduce sales and lead to decreasing profits.

However, DG systems inherently provide some benefits to the utility. They may level the load curve, improve the voltage profile across the feeder, may reduce the loading level of branches and substation transformers, and provide environmental benefits by offsetting the pollutant emissions [1]. Utility economic benefits also include loss reduction, avoided costs of energy production, generation capacity, distribution and transmission capacity investment deferral, reducing risk from uncertain fuel prices, green pricing benefits, etc.

Usually, PV systems are designed to operate at unity power factor, providing only active power to the utility. This design maximizes the benefits of the individual customer, since residential customers are usually charged only for the active power that they draw from the grid. However, PV systems may be operated at non-unity power factor, and there are situations when it is reasonable to allow PV systems to generate limited amounts of reactive energy. The utility regulations [2] dictate that PV systems should operate at a power factor greater than 0.85 (leading or lagging), when output is greater than 10% of rating, but specially designed systems that provide reactive compensation or voltage support may operate outside of this limit with utility approval.

2. Problem description

The following paragraph illustrates the effect of DG penetration on the actual load demand and voltage profile of the distribution feeder equipped with switched shunt capacitors. In radial networks, bus voltages decrease as the distance from the distribution transformer increases, and may become lower than the minimum voltage permitted by the utility. Utilities usually combat this problem by increasing the tap ratio of the distribution transformer, and/or by switching on the shunt capacitors. By providing a portion of energy on site, DG systems reduce branch currents, which in turn leads to reduced losses and increased voltage throughout the feeder.

We will consider the 69-bus, 8-lateral distribution feeder, based on the data from [3], with few modifications concerning the placement of loads. The feeder lateral layout is shown in Fig. 1; the locations of loads, shunt capacitors and one possible distribution of PV generators are also shown.

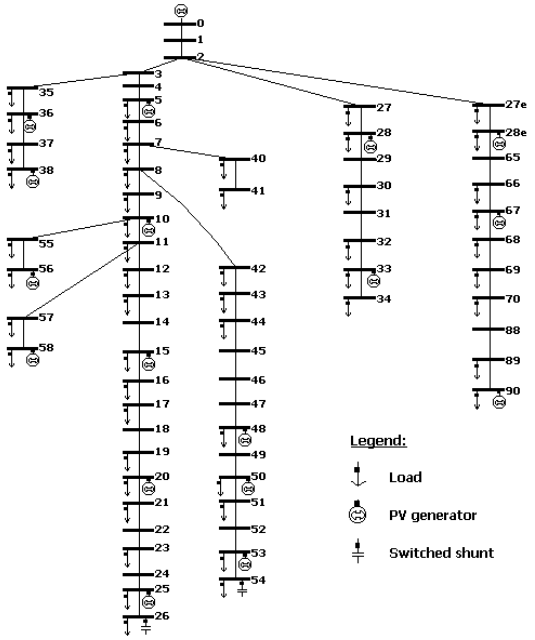

Fig. 1. The test system [3].

The lowest voltage for a base case without compensation is 0.94 at bus 54 for a summer day with heavy load. Using sensitivity analysis buses 26 and 54 were identified as best places to add reactive shunt support. The shunts considered are standard discrete blocks of 0.3MVAr controlled locally using simple low/high voltage limit regulations, which connect the necessary number of blocks in order to maintain controlled voltage between low and high threshold levels.

PV generators scattered across the feeder and operating at unity power factor behave as a negative active load, effectively decreasing the load active power demand (Fig. 2a - Fig. 4a), and thus improving local voltage conditions (Fig. 2b - Fig. 4b). The capacity of PV generators scattered across the feeder as shown in Fig. 1, was scaled from 0% to 40% of local loads at their respective buses.

Fig. 2b shows the voltage at a remote feeder bus for a typical sunny day with high load demand. Without PV support, the shunt capacitors are turned on early in the morning as the load demand increases and voltage drops below the threshold level. PV generators improve the voltage profile, but just delay the turn-on of the switched shunt, since the PV and load profile characteristics are not closely matched. While the PV generation peaks around noon, the peak of the load demand occurs at sunset when PV generation is not capable of maintaining the voltage above the threshold value (0.95 p.u.). Similar situation is portrayed in Fig. 3. Without PV support, the capacitors turn on at 10:00am, but even 10% PV support is enough to keep the voltage above 0.95. However, since the load peak occurs after dark, when PV generators are not active, the voltage profile worsens and the shunt capacitors turn on. Note that this might have been avoided if the PV system was equipped with battery storage (expensive solution), or if the PV and load characteristics were better matched. Fig. 4 illustrates that situation. Both PV and load peaks occur around 11:00am. Even a moderate 10% PV support is quite enough to keep the voltage within the acceptable limits throughout the day; the shunt capacitor never turns on.

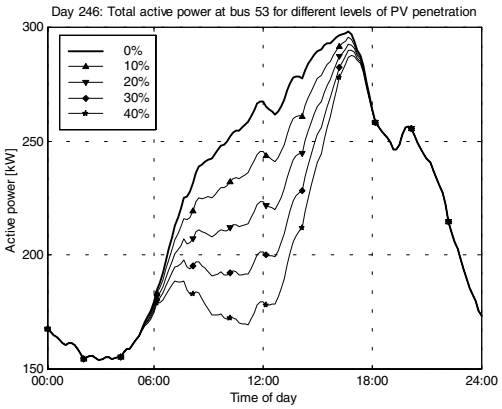

a) Active power at bus 53

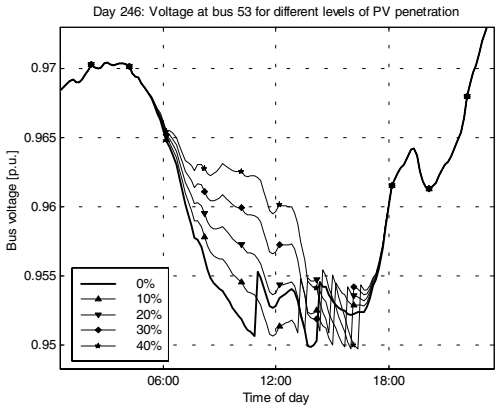

b) Voltage at bus 53

Fig. 2. Effects of PV generation - sunny day with high load. PV provides only active power.

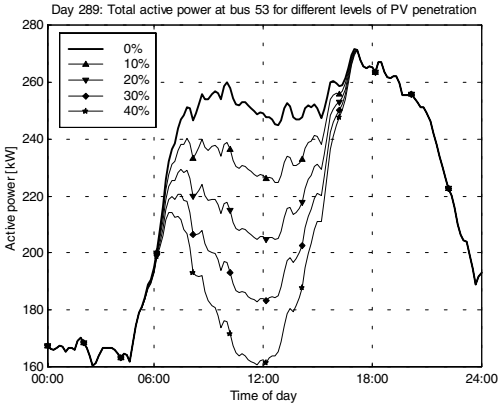

a) Active power at bus 53

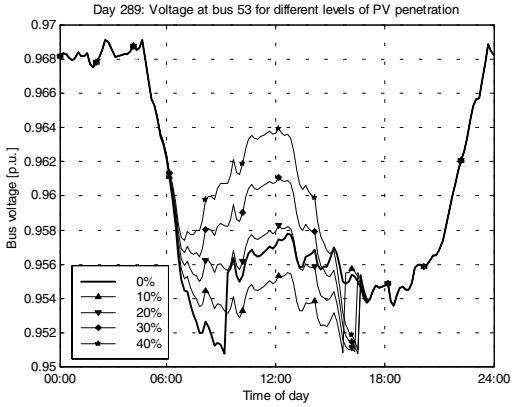

b) Voltage at bus 53

Fig. 3. Effects of PV generation - typical fall day. PV provides only active power.

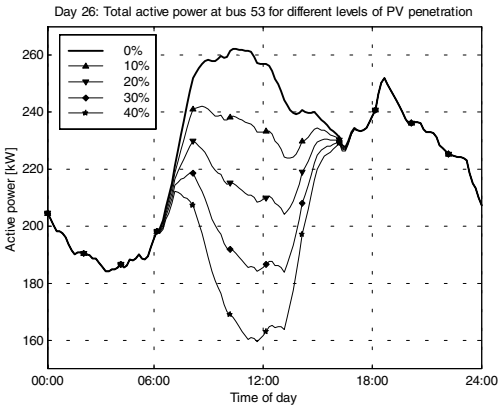

a) Active power at bus 53

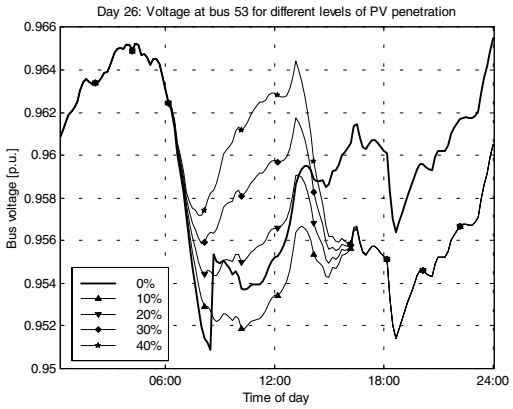

b) Voltage at bus 53

Fig. 4. Effects of PV generation - sunny day with moderate load. PV provides only active power.

3. DG-enhanced feeder operation

The above figures provide only the qualitative analysis of the effect that DG systems may have on the operation of the distribution feeder. We now present a systematical study which attempts to quantify these and several others aspects of the DG-enhanced feeder operation.

3.1 Load and PV profiles

We use the test system shown in Fig. 1, for which the hypothetical daily load profile is obtained from the actual utility data for a Central-US small city. The measured utility data spans one whole year in 10-minute intervals, which is also the period considered in this study. It is assumed that all of the loads at the feeder follow the same active and reactive load patterns, however, those patterns are different for active and reactive power consumption.

The PV generation was obtained by simulating an ideally oriented and tilted fixed 1kW PV system at the actual Central-US location using PV simulation program PVGRID 7.1. The following derating coefficients were used: shading 4%, dust 4%, mismatch 2%, DC losses 2%, MPPT losses 4% and the inverter efficiency was assumed to be 93%. This approach allows simple scaling of a system, by simply multiplying the energy output values by the nominal power of the actual system. Non-optimally oriented and tilted systems may be simulated by multiplying the output of the system by a number smaller than one. The output of PVGRID is obtained in hourly intervals and linearly interpolated to get the PV production in 10-minute intervals. The weather input to PVGRID was derived from the TMY2 database that serves as a standard database for weather conditions in the US [4].

3.2 Inverter control strategies

In the case of renewable DG systems, the DC energy obtained from the renewable source is fed through the power-conditioning unit (inverter). The majority of contemporary inverters used in DG systems are current source inverters (CSI) operating at unity power factor, and hence the overall power factor of a distribution feeder enhanced by DG and equipped with such inverters would be lower. If, however, we assume that voltage source inverters (VSI) can be utilized instead of CSI, we can generate reactive power commensurate with the remaining unused capacity at any given point in time, as shown in Fig. 5.

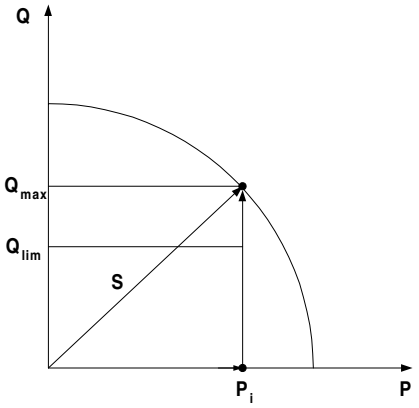

Fig. 5. The inverter modes of operation.

The active power output of the inverter P_i is determined by the amount of power that is supplied by PV modules, and inverter's efficiency. The majority of DG inverters supply only active power, however, there is no intrinsic barrier for inverters to supply reactive energy as well. For a given active power output P_i, the inverter's reactive power output Q_i is limited by its nominal apparent power rating S, i.e. can be anywhere between zero and Q_{max}, as shown in Fig. 5. The current regulations dictate that PV inverters should operate with power factor above 0.85 [2], but specially designed systems may operate with lower power factor with utility's approval. The reactive limit Q_{lim} determined by this power factor condition is also shown in Fig. 5. In addition, the inverter's reactive output is limited by the maximum allowable voltage at its bus. The size of the inverter is dictated by the maximum expected DC power over a prolonged period of operation. In the case of PV, or wind DG systems, the supplied DC power is determined by the available solar or wind energy at that time point. The actual DC power and inverter's active power output will therefore typically be less than the inverter's apparent power rating S, which provides plenty of opportunities for the reactive power output. As an example, Fig. 6 shows the histogram of the annual active energy production of the 2kW PV system equipped with 2kVA inverter, and corresponding histograms of the maximum reactive annual energy output of that inverter for cases when its reactive power output is limited by Q_{max} and Q_{lim}, as explained above. The PV production was obtained using PVGRID 7.1 and TMY2 database.

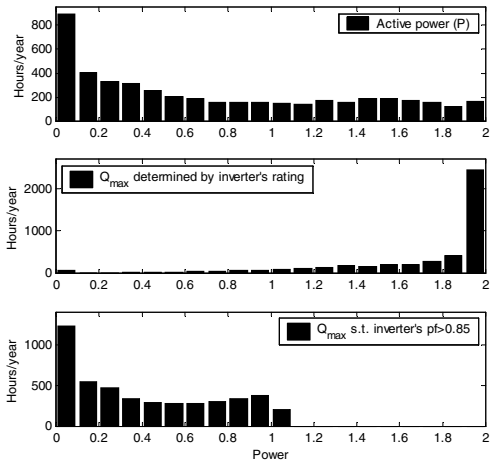

Fig. 6. Histograms of annual inverter active energy production and corresponding reactive production, limited by Q_{max} and Q_{lim}.

We will consider the following inverter control strategies:

1. Inverter supplies only active power:

$$P_i = \eta P_{DC}, Q_i = 0 \quad (1)$$

2. Same as 1), but inverter also supplies maximum available reactive power up to the limit Q_V determined by the maximum allowable voltage at its bus:

$$P_i = \eta P_{DC}, Q_i = \min(Q_V, Q_{\max}) \quad (2)$$

3. Same as 2), but under constraint that its power factor is above 0.85.

$$P_i = \eta P_{DC}, Q_i = \min(Q_V, Q_{\lim}) \quad (3)$$

3.3 DG systems placement

The utility usually does not have the apriori knowledge of the locations and sizes of small distributed DG systems (usually PV and/or wind systems) across its feeder. Therefore, it is beneficial for it to know the boundaries that a specific DG feeder penetration will have on some specific quantities of interest, such as voltage profile,

active and reactive losses, and switching times of shunt capacitors. The utility would also be interested in knowing the exact locations that will provide best overall impact on the feeder, in terms of those quantities.

We will consider four different PV penetrations: 190kW, 380 kW, 570kW and 760kW, which represent approximately 5%, 10%, 15% and 20% of the total feeder load. We assume that all PV systems are multiples of the standard PV "building block" of 2kW, i.e. for a 760kW PV penetration, 380 "building blocks" are scattered across the feeder. In order to conserve space, only the results for 760kW feeder penetration are presented; the results for remaining feeder penetrations are, as expected, appropriately lower.

Two different random spatial distributions were considered for determining the PV generator locations: uniform and Poisson. Uniform distribution tends to spread PV generators evenly across the feeder. Result is that for a fixed penetration level, almost all load buses have relatively small PV systems connected to them. Using the Poisson distribution with a suitable parameter λ, we can force that the same total PV power is spread over fewer load buses. Therefore, the PV capacity on those buses will be higher. Using the Poisson distribution, but restricting the generators to be spread to a maximum of 60% of the load buses, we are imposing a situation with very few, relatively large DG systems across the feeder. Fig. 7 shows one possible PV generator placement in those three cases for the total feeder penetration level of 760kW.

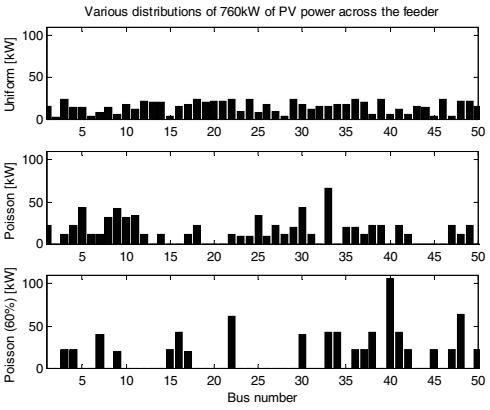

Fig. 7. PV generators placements throughout the feeder for uniform and Poisson distributions.

4. Performance analysis using clustering techniques

In order to fully determine the actual effects of the random placement of PV systems throughout the feeder, the daily and annual variations of the DG performance have to be accounted for. At first, 500 series of yearly Monte Carlo simulations have been proposed. Each simulation should have identical load conditions, but different PV generator locations and sizes according to the chosen PV spatial distribution (uniform or Poisson). The whole procedure should be repeated for three considered inverter strategies. This is a very computer-intensive process, considering that a total of 26,280,000 (6 24 365 500) power flow solutions would have to be calculated for each spatial PV feeder distribution and inverter control strategy. Even if we restrict the data set to include only daytime-hours, more than 14,000,000 simulations would be needed. Alternatively, we could use just several typical days, but by doing so, important annual aggregate values would be lost.

We are proposing a different strategy. Instead of using a complete annual data set or just a couple of typical days, let us extract the smaller set of points that can actually represent the behavior of the feeder with PV penetration throughout the year. The mathematical representation follows.

Let X be our data set composed of all daytime vectors x_i of active (P_i), reactive (Q_i) and PV (P_{PVi}) power throughout the year, i.e.:

$$X = \left\{ x_i \mid x_i = \left(P_i, Q_i, P_{PV_i} \right),\ i = 1,\ldots, N \right\} \tag{4}$$

Define set D as a smallest set that contains set X. The objective is to generate set M with minimal number of elements such that:

$$M = \left\{ y_i \mid y_i \in D,\ y_i \text{ represents D accurately} \right\} \tag{5}$$

where the statement "accurate representation" means a suitably chosen mathematical criterion, which will be defined later in the text. One method to generate set M is to perform the cluster analysis of the set X. Clustering algorithms identify natural groupings of data in a large data set, sorting the data into several groups (clusters), which can then be processed as single entities. The conventional clustering algorithms assign each data point to only one cluster. The m-clustering of a set X is defined as a partition of X into m sets $C_1,\ldots,C_m$, where the following conditions are met:

$$\begin{aligned} &(1)\ C_i \neq \phi,\ i = 1,\ldots, m \\ &(2)\ \bigcup_{i=1}^{m} C_i = X \\ &(3)\ C_i \cap C_j = \phi,\ i \neq j,\ \ i, j = 1,\ldots, m \end{aligned} \tag{6}$$

In other words, there cannot be zero-clusters (1), missed data (2), or overlapping clusters (3). In fuzzy clustering algorithms, each data point x_i belongs to cluster C_j to some degree specified by its membership grade u_{ij}. The fuzzy clustering of X into m clusters is defined by a mxN membership matrix U whose elements are membership grades u_{ij} if the following conditions are met:

$$\begin{aligned}
&(1)\ u_{ij} : X \to [0,1],\ i = 1,...,N,\ j = 1,...,m \\
&(2)\ \sum_{j=1}^{m} u_{ij} = 1,\ i = 1,...,N \\
&(3)\ 0 < \sum_{i=1}^{N} u_{ij} < N,\ \mathrm{j} = 1,...,m
\end{aligned} \tag{7}$$

The membership grades close to unity indicate a "high grade" of membership to the corresponding cluster. It can be proven that the conventional “hard” clustering can be considered as a special case of fuzzy clustering, with membership grades restricted to take values only from $\{0,1\}$.

In order to separate data into clusters, a proximity measure between data vectors and between a point and a cluster needs to be defined:

$$d(x_i, x_j) = \left\| f(x_i) - f(x_j) \right\| \tag{8}$$

where f is a suitably chosen function. One commonly used proximity measure between two vectors is the standard Euclidean distance, where $f(x)=x$. Each cluster can be represented by a simple vector, called the point representative of the cluster and denoted as w_j. Therefore, the distance between the vector and a cluster can be calculated as a distance between the vector and the cluster point representative. The objective of the clustering algorithm is then simply to obtain the cluster’s point representatives w_j and membership matrix U. This is done by minimizing the cost function of the form

$$J_q(W,U) = \sum_{i=1}^{N} \sum_{j=1}^{m} u_{ij}^q d(x_i, w_j) \tag{9}$$

with respect to W and U, subject to the constrains for membership grades u_{ij} presented above. The parameter q is called a fuzzifier ($q>1$) and the matrix W is defined as

$$W = \left[w_1^T, ..., w_m^T \right]^T \tag{10}$$

This approach leads us to the Lagrangian in the following form:

$$L(W,U) = \sum_{i=1}^{N} \sum_{j=1}^{m} u_{ij}^q \cdot d(x_i, w_j) - \sum_{i=1}^{N} \lambda_i \left(\sum_{j=1}^{m} u_{ij} - 1 \right) \tag{11}$$

Using standard minimization techniques, we arrive at the following two equations:

$$\begin{aligned}
u_{ij} &= \frac{1}{\sum_{k=1}^{m} \left(\frac{d(x_i, w_j)}{d(x_i, w_k)} \right)^{\frac{1}{q-1}}},\ i = 1,...,N,\ j = 1,...,m \\
\sum_{i=1}^{N} u_{ij}^q \frac{\partial d(x_i, w_j)}{\partial w_j} &= 0,\ j = 1,...,m
\end{aligned} \tag{12}$$

These equations are coupled and cannot, in general, yield a closed form solution. They are solved iteratively, by taking an initial guess for the cluster point representatives matrix W, calculating the membership matrix U, updating W, and continuing this process until the termination criterion is reached. In the case of hard clustering, the equations simplify significantly, since u_{ij} is restricted to only two values (0 or 1). Hard clustering algorithms, however, tend to have problems with non-compact clusters usually found in real-life data. The main advantage of fuzzy clustering is that it captures the imprecision encountered when describing real-life data, providing more information about the data structure compared to a non-fuzzy scheme. We have employed a fuzzy c-means (FCM) clustering algorithm that uses the squared Euclidean distance as a proximity measure and a value $q=2$ for the fuzzification parameter.

The drawback of the fuzzy clustering algorithm is that it requires the number of clusters to be known in advance. However, several validity criteria can be used to determine the optimal number of clusters, once the clustering is performed [5]. They measure the quality of clustering by assigning the value to it. The more the data points are concentrated around the cluster centers, the cluster structure is better and the criteria values are lower. The Xie-Beni (XB) index is used for validation of clustering produced by the fuzzy-c means algorithm when the Euclidean distance is in use, and can be calculated as

$$XB = \frac{J_2}{N \cdot D_{\min}^2} \tag{13}$$

where J_2 is the cost function defined in (9), N is the number of data vectors, D_{min} is the minimum Euclidean distance between two cluster point representatives, i.e.

$$D_{\min} = \min_{\substack{i,j=1,\ldots,m \\ i \neq j}} \left\| w_i - w_j \right\| \quad (14)$$

m is the number of clusters and w_k is a vector defining the point representative of the cluster k. Note that the *XB* index is a monotonically decreasing function of the number of clusters m, as m gets close to N, indicating that in that range the *XB* index is not a valid fuzzy clustering validity criterion [6]. However, the optimal value m_{opt} is much smaller than N, and we will not reach the starting point of the decreasing tendency. The optimal number of clusters can be found by examining the plot of *XB* as a function of m, which is shown in Fig. 8.

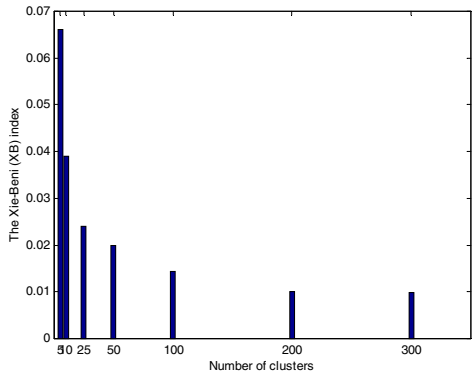

Fig. 8. The Xie-Beni index as a function of number of clusters.

The structure of *XB* index in Fig. 8 indicates that the benefit of increasing the number of clusters rapidly decreases after a certain number of clusters is reached (1-200), which can be used as a criterion for the selection of optimal number of clusters. We have chosen the optimal number of clusters as m_{opt}=200. Since the total number of data vectors is N=*28137*, this value is well below the range where m and N are comparable.

The point representatives of these *200* clusters form the set M that will be used for Monte Carlo simulations. The scatter plots of all data vectors with superimposed cluster point representatives shown in Fig. 9 and Fig. 10 reveal that the clustering algorithm has indeed maintained the intrinsic data structure. Note however that *XB* index only validates the goodness of clustering; it does not guarantee that the results of analysis using the reduced clustered set will provide an accurate description of the actual feeder behavior.

The cluster point representatives are also shown sorted by the load active power in Fig. 11, which shows significant correlation between P and Q (as expected), but no correlation between P and P_{PV}, indicating that all the computational effort we are undertaking is in fact required.

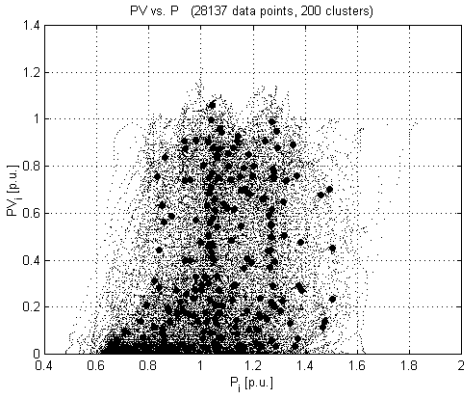

Fig. 9. The data and cluster center points (projection onto the PV-P plane).

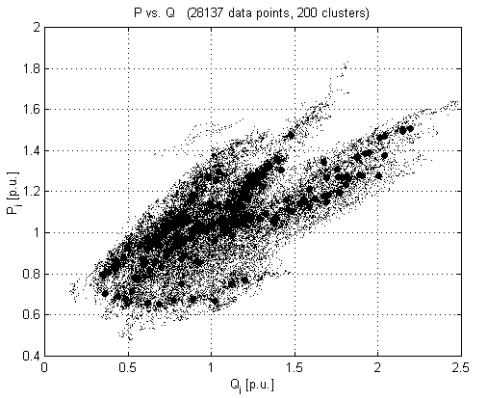

Fig. 10. The data and cluster center points (projection onto the P-Q plane).

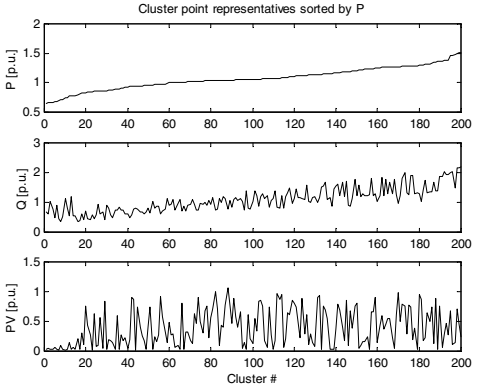

Fig. 11. Cluster point representatives (*m=200*).

In order to validate that the analysis using the reduced clustered set will in fact provide dependable results, we

have simulated a full year of feeder operation for a particular PV placement distribution and inverter control strategy using all available daytime-hours data points and compared the results to the results obtained using only cluster centers for several clustering scenarios. Table 1 shows the total annual consumption, losses and total number of shunt capacitor control (on/off) actions for the DG-equipped feeder using cluster sizes of *10*, *20* and *28137* (all data points). All quantities (losses, total consumption, number of switch shunt control actions) are expressed as a percentage of quantities calculated without DG support. The results indicate that reductions in total cumulative annual feeder energy consumption and losses obtained by placing DG throughout the feeder can be estimated using relatively small number of clusters. However, more accurate clustering is needed to investigate the effects of DG penetration on the operation of switched shunt capacitors.

Table 1. Total feeder consumption, losses and number of shunt capacitor control actions.

Cluster size		10	200	28137
Losses	P [%]	83.34	82.37	82.88
	Q [%]	84.63	83.83	84.27
Feeder consumption	P [%]	92.5	92.46	92.74
	Q [%]	46.76	42.23	40.92
Switchings	[%]	37.5	55.4	51.91

Fig. 12 shows the substation-level power factor duration curves for the same three clustering scenarios. The solid line, obtained using 200 cluster center points, closely tracks the bold solid line obtained using all 28137 data points, while the curve obtained with only 10 cluster center points shows significant discrepancies from the bold curve, indicating that more than 10 clusters are needed for accurate modeling of feeder operation.

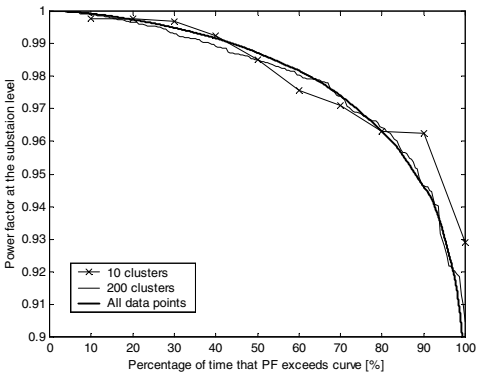

Fig. 12. Power factor duration curve for several clustering scenarios.

5. Monte Carlo analysis

Five hundred Monte Carlo simulations have been performed using 200 cluster point representatives for each considered PV spatial distribution and inverter control strategy. Fig. 13 and Fig. 14 show the minimum, average and maximum recorded values for the substation-level power factor and remote bus voltage duration curves for two PV spatial distributions, assuming that the inverter's reactive power output is limited by its kVA limit. Although the range of recorded values for both power factor and voltage is, as expected, wider in the case of Poisson distribution, the average values (solid lines) are almost identical. The improvements, compared to the base case without DG (bold solid line) are clearly noticeable. Poisson distribution yields slightly better maximum voltage improvement, showing that it may be advantageous to concentrate PV systems on buses where low voltages are expected. The average values can be used for simple cost-benefit calculations.

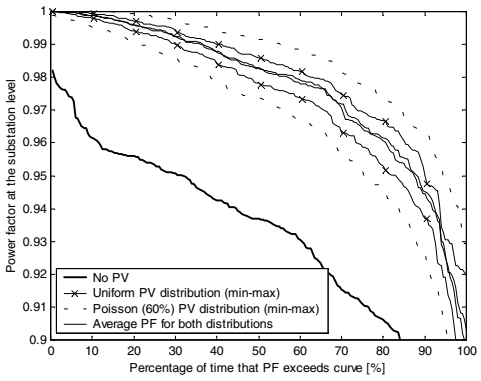

Fig. 13. Power factor duration curves for different PV spatial distributions.

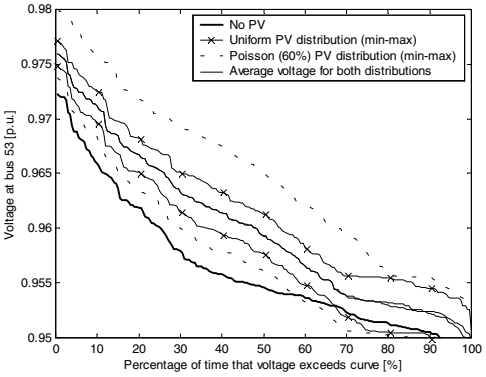

Fig. 14. Voltage duration curves for different PV spatial distributions (bus 53).

The average and extreme values of total distribution feeder losses, total energy taken from the transmission network and the total number of shunt capacitor control (on/off) actions over 500 Monte Carlo simulations for a total PV penetration of 760KW are summarized in Table 2. All three quantities are expressed as a percentage of the values that were calculated without PV support, showing the improvement obtained by PV penetration. Without PV, the active and reactive losses are 1.72% and 2.28% of the total active and reactive energy taken from the transmission system throughout the year, respectively. Table 2 depicts results obtained for all considered spatial PV system distributions (uniform and Poisson), and all inverter control strategies (supplying only active power, both active and reactive but limiting inverter power factor to be higher than 0.85, and supplying reactive power up to the maximum allowable by the kVA inverter rating).

Table 2. Total feeder losses, energy consumption and number of shunt control actions over 500 Monte Carlo simulations for different PV spatial distributions and inverter control strategies.

Total penetration: 760kW (~20%)			Losses		Feeder consumption		Switchings
			P [%]	Q [%]	P [%]	Q [%]	[%]
Uniform PV distribution	No Q generated	Min	86.05	87.44	92.52	101.80	64.75
		Avg	88.06	89.04	92.55	102.75	74.55
		Max	90.30	90.77	92.59	103.89	82.73
	Max Q subject to pf>0.85	Min	83.31	84.48	92.47	90.67	59.71
		Avg	85.67	86.82	92.51	91.98	67.20
		Max	88.19	88.89	92.56	92.83	78.42
	Max Q allowed by kVA rating	Min	77.02	78.98	92.36	41.78	32.37
		Avg	79.98	81.32	92.42	46.33	46.01
		Max	83.14	84.10	92.47	50.81	64.03
Poisson PV distribution	No Q generated	Min	84.51	86.11	92.49	101.34	58.27
		Avg	88.20	89.15	92.56	102.73	74.74
		Max	93.31	93.32	92.64	104.60	87.05
	Max Q subject to pf>0.85	Min	81.00	82.93	92.43	90.18	48.92
		Avg	85.81	86.92	92.52	91.91	67.76
		Max	91.85	91.84	92.62	94.06	82.73
	Max Q allowed by kVA rating	Min	74.25	76.61	92.32	39.11	19.42
		Avg	80.30	81.58	92.42	46.15	46.92
		Max	88.62	88.50	92.56	54.15	70.50
Poisson PV distribution (only 60%)	No Q generated	Min	81.80	84.31	92.45	101.11	56.12
		Avg	88.27	89.20	92.56	102.70	74.95
		Max	94.38	94.46	92.66	104.81	89.21
	Max Q subject to pf>0.85	Min	78.08	81.10	92.38	89.74	46.76
		Avg	85.85	86.95	92.52	91.82	68.55
		Max	92.39	93.37	92.64	94.27	87.05
	Max Q allowed by kVA rating	Min	72.71	74.96	92.28	35.21	15.83
		Avg	80.84	82.01	92.43	45.17	47.82
		Max	89.78	90.43	92.58	57.24	76.98

The obtained results verify that PV penetration actually enhances the feeder condition by reducing losses, improving the power factor and enhancing the voltage profile. Thus, voltage stability of the system that supplies energy to the feeder is also improved.

6. Conclusions

The performance assessment of the DG-equipped feeder is a challenging problem at the planning stage, because of the uncertainties involved in both predicting the DG placement and its future operation. We approach the problem from the statistical standpoint and identify the features that allow significant reduction of the computation involved while retaining the important information in the input data.

In the illustrations used to demonstrate the salient features of the proposed approach, we also investigate the impact of DG grid-connected inverter control on feeder voltage performance. This may be used in the future to enhance voltage stability of the feeder and the network it is connected to, which is the subject of ongoing investigation.

7. References

[1] T. Hoff, D. S. Shugar, "The Value of Grid-Support Photovoltaics in Reducing Distribution System Losses", *IEEE Transactions on Energy Conversion*, Vol. 10, No. 3, September 1995, pp 569-576.

[2] "*Recommended Practice for Utility Interface of Photovoltaic (PV) Systems*", IEEE 929-2000 Standard, 2000.

[3] M. E. Baran, F. F. Wu, "Optimal Capacitor Placement on Radial Distribution Systems", *IEEE Transactions on Power Delivery*, Vol. 4, No. 1, January 1989, pp. 725-732.

[4] W. Marion, K. Urban, "*User's Manual for TMY2s*", National Renewable Energy Laboratory, June 1995.

[5] S. Theodoridis, K. Koutroumbas, "*Pattern recognition*", Academic Press, 1999.

[6] Xie. X. L., Beni. G, "A validity measure for fuzzy clustering", *IEEE Transactions on Pattern Analysis and Machine Intelligence*, Vol. 13, Issue 8, 1991, pp. 841-846.